JANUARY 1981 PPPL-1740
UC-20f
CONF-810707--25

PDX EXPERIMENTAL RESULTS

PLASMA PHYSICS LABORATORY

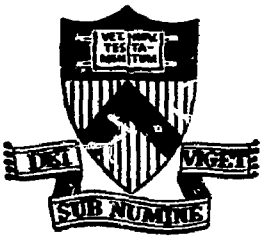

PRINCETON UNIVERSITY
PRINCETON, NEW JERSEY

This work was supported by the U.S. Department of Energy Contract No. DE-AC02-76-CHO 3073. Reproduction, translation, publication, use and disposal, in whole or in part, by or for the United States government is permitted.

PDX EXPERIMENTAL RESULTS

D. MEADE, V. ARUNASALAM, C. BARNES, M. BELL, K. BOL, M. BITTER, R. BUDNY, J. CECCHI, S. COHEN, C. DAUGHNEY, S. DAVIS, D. DIMOCK, F. DYLLA, P. EFTHIMION, H. EUBANK, R. FONCK, R. GOLDSTON, B. GREK, R. HAWRYLUK, E. HINNOV, H. HSUAN, M. IRIE*, R. JACOBSEN, D. JOHNSON, L. JOHNSON, H. KUGEL, H. MAEDA**, D. MANSFIELD, R. McCANN, D. McCUNE, K. McGUIRE, D. MIKKELSON, S. MILORA†, D. MANOS, D. MUELLER, M. OKABAYASHI, K. OWENS, M. REUSCH, K. SATO, N. SAUTHOFF, G. SCHMIDT, J. SCHMIDT, E. SILVER, J. SINNIS, J. STRACHAN, S. SUCKEWER, H. TAKAHASHI, F. TENNEY

Plasma Physics Laboratory, Princeton University

Princeton, New Jersey 08544 USA

* University of Waseda, Tokyo, Japan

** Japan Atomic Energy Research Institute, Tokai, Japan

† Oak Ridge National Laboratory, Oak Ridge, Tennessee, USA

Paper presented at the 8th International Conference on Plasma Physics and Controlled Thermonuclear Fusion Research, Brussels, 1-10 July 1980, Paper IAEA-CN-38/X-1.

ABSTRACT

During the initial period of operation PDX has obtained the following results:

- Production of macroscopically stable poloidal divertor configurations with Dee, inverse-Dee and single null plasma shapes.
- Determined vertical positional instability growth rates for passively stabilized elongated Dee shaped plasmas with surface elongations from 1 to 1.4.
- Production of $Z \simeq 1$ plasmas in a diverted Dee configuration with confinement times approaching 80 ms for plasmas with $I_p \simeq 300$ kA, $B_T = 17$ kG, $a \simeq 38$ cm, $q \simeq 3$ and $\bar{n}_e \simeq 4 \times 10^{13}$ cm^{-3}.
- Extended the ohmic heating regime to $q \simeq 2$ at $\bar{n}_e R/B_T \simeq 10^{15}$ cm^{-2}T^{-1} and $q \simeq 3$ at $\bar{n}_e R/B_T \simeq 4.5 \times 10^{15}$ cm^{-2}T^{-1}. Neutral beam injection has extended $\bar{n}_e R/B_T$ to $\sim 6 \times 10^{15}$ cm^{-2}T^{-1}.
- Initial neutral beam injection experiments with 1 - 2 MW injected perpendicularly have been used to study ion and electron heating with divertor control of density and impurities.
- Divertor physics studies indicate that the divertor captures ~70% of the input power, while ~30% of the power is radiated.
- Particle and energy flow onto the divertor neutralizer plate is in qualitative agreement with a simple sheath model.

1. INTRODUCTION

The main objectives of the Poloidal Divertor Experiment (PDX) are to:

- determine the effectiveness of poloidal divertors in controlling impurities in high temperature plasmas,
- use the poloidal divertor to provide clean plasmas for confinement and high beta studies and
- investigate the effect of cross-section shaping on plasma confinement and MHD properties.

In this paper, we report the results obtained during initial divertor operation of the PDX.

2. DESCRIPTION OF THE PDX DEVICE

Figure 1 shows a cross-sectional schematic of the PDX device. The main design parameters are: R = 130 - 150 cm, a ≃ 40 cm, B_T = 25 kG and I_p = 500 kA for a 1 s pulse [1,2] . During operation so far, the fields and currents have been run at 2/3 their design values. All surfaces in contact with the plasma (limiters, divertor neutralizer plates and baffles) are made from 99% pure titanium. The vacuum vessel is pumped by turbopumps with a speed of 3 kℓ/s for H_2. During operation, ten titanium evaporators getter half of the twenty divertor burial chamber cells providing a pumping speed of ~200kℓ/s for H_2 and base pressures ~10^{-8} Torr.

3. MAGNETIC PROPERTIES OF PDX DISCHARGES

3.1 Discharge Initiation and MHD Equilibrium. The magnetic system of PDX was designed to produce, with the divertor windings energized, an initial quasi-static hexapole magnetic null at a small major radius to form the discharge away from metallic limiters. However, it has been found that transient fields

generated by currents induced in the toroidally continuous vacuum jackets of the internal divertor coils are of predominant importance during startup. Although, in practice, a very good octopole null can be created near the vacuum vessel center by cancelling the divertor and eddy current fields with a small applied dipole field, present indications are that plasma current buildup occurs more readily when the applied field is adjusted to produce a radially stabilizing quadrupole null at a radius of about 160 cm. While the current buildup from 20 to 100 kA is extremely sensitive to the applied vertical field and its rate of rise, with careful programming of the field and feedback position control, discharges can be started reproducibly.

Typical MHD equilibria obtained in PDX during the current flattop are shown in Fig. 2; these computed flux plots satisfy as boundary conditions the plasma and coil currents, and the vertical magnetic field measured at a point above the plasma. The plasma can be moved from one configuration to another continuously by varying the vertical field and thereby changing the radius of the magnetic axis, R_m. The calculated position of the divertor separatrix for the standard-Dee is in agreement with the position at which the outside movable limiter cuts off the flow to the divertor and the transition from Dee to inverse-Dee with variation of R_m has been verified experimentally with microwave interferometers in the divertor channels.

3.2 Vertical Positional Stability. Pairs of divertor coils that are mirror symmetric about the midplane are connected in parallel, and these parallel units are then connected in series to the divertor power supply. This creates an effective copper shell that can passively stabilize vertical plasma motion. In PDX, the vacuum field index ($n_v = -R/B(\partial B/\partial R)$) is a function of the major radius of the plasma (Fig. 3). Thus, the plasma elongation near the separatrix is also a function of major radius with $\varepsilon \approx 1.0$ at $R_m = 140$ cm and

$\varepsilon \simeq 1.4$ for a Dee at $R_m = 120$ cm or an inverse-Dee at $R_m = 170$ cm (ε is the ratio of the axial to major radial diameters of the surface containing 95% of the total poloidal flux within the separatrix).

The stabilizing effect of the divertor coils was estimated by assuming a simple rigid plasma displacement and calculating the radial field due to the currents induced in the passive stabilization circuit, expressing the result as an additional effective field index, n_{ps}: for $n_v > 0$ the plasma is vertically (n = 0, m = 1) MHD stable, for $n_v + n_{ps} > 0$ it is passively stabilized and for $n_v + n_{ps} < 0$ it is unstable. The passively stabilized case has a calculated growth rate as shown in Fig. 3. These criteria were tested by creating a stable discharge at $R_m \simeq 140$ cm and then varying the plasma major radius to a new value during the pulse (Fig. 3). The vertical plasma position was measured as a function of time, and a growth rate was determined. The measured growth rate shows reasonable agreement with the predictions of the simple model. In these experiments a maximum elongation of $\varepsilon \simeq 1.4$ was obtained for a passively stabilized discharge. The difference between the measured and predicted growth rates may be due to differences between the assumed and actual current profiles or to the fact that the plasma may not be perfectly rigid during a vertical displacement. Only limited vertical stability studies of an elongated inverse-Dee were made since the inverse-Dee became disruptive before significant elongations were obtained. Whether this is a result of intrinsic plasma instability or impurity behavior will be the subject of future experiments.

3.3 MHD Fluctuations. Theoretically, we expect the MHD stability to be a function of the external field configuration as well as the current and pressure profiles [3,4]. Since impurities are also dependent on the external configuration and can influence the current profile, it is very difficult to draw conclusions on the correlation between MHD activity and the magnetic

configuration. In general, standard-Dee configurations have a relatively low level of impurities and are characterized by a low level of m = 2 activity and 10% sawtooth oscillations in the electron temperature with periods of 5 - 15 ms. These discharges run reproducibly and stably at $q_a \approx 3.1$ ('q_a' is the safety factor calculated for an equivalent circular plasma); the minimum 'q_a' obtained in the Dee configuration was 2.1. Major disruptions have resulted in a total current decay time as short as 5 ms although typical disruptions are longer. Circular discharges with a titanium limiter have a larger impurity content and under our present conditions are more likely to have m = 2 activity than the divertor discharges. However, stable circular discharges with sawtooth activity have also been routinely produced. Slightly inverse-Dee configurations which are between those shown in Figs. 2c and 2d are macroscopically stable and have MHD fluctuation levels between those of the Dee and circular plasmas.

4. PROPERTIES OF OHMICALLY HEATED DISCHARGES

4.1 Operating Parameter Range. Following the approach of Stott et al. [5] typical parameters for ohmically heated PDX discharges are shown in Fig. 4. High electron densities are usually achieved by programming the gas injection feedback system to produce a steady rise for 700 ms followed by a 300 ms flattop. The maximum density obtained with ohmic heating corresponds to a Murakami parameter [6] $\bar{n}_e R/B_T \approx 4.5 \times 10^{15}$ cm^{-2}T^{-1}. Neutral beam injection of 1 - 2 MW permits stronger gas puffing which has produced a maximum density corresponding to $\bar{n}_e R/B_T \approx 6.5 \times 10^{15}$ cm^{-2}T^{-1}. By terminating the gas puffing before the end of the beam pulse, the density can be brought down rapidly in the divertor discharges to a level that can then be sustained without disruption by the ohmic heating alone.

4.2 Confinement of Ohmically Heated Discharges. The evolutions of electron density, plasma current and radial position are controlled by feedback systems on the gas injection valves and poloidal field power supplies. These systems are especially useful in obtaining reproducible discharges for parameter studies of energy confinement and comparisons of different magnetic configurations. The electron temperature profile is measured primarily with a 5 chord soft x-ray pulse height analyzer system. For circular discharges, the electron temperature inferred from electron cyclotron emission is in agreement with the x-ray measurements for both magnitude and profile shape [1]. Within the experimental uncertainties, initial results from Thomson scattering also support the x-ray measurements. Ion temperatures are determined from a 2 chord 10 energy channel charge exchange system, Doppler broadening of impurity lines, and neutron emission in the case of deuterium plasmas. Electron density profiles are measured with a two dimensional 9 chord 2 mm microwave interferometer and appear to be somewhat flatter than parabolic. An infrared methyl alcohol laser interferometer is used to extend the microwave density measurements to higher densities.

The electron energy confinement time τ_{Ee} is defined by

$$\frac{d}{dt} E_e = - \frac{E_e}{\tau_{Ee}} + P_{OH} \quad , \quad E_e = \int \frac{3}{2} n_e k T_e dV \quad . \quad (1)$$

The ohmic power input is determined by solving a one dimensional magnetic field diffusion equation for $j(r)$ subject to the constraints of the measured I_p and V_ℓ. Neoclassical resistivity [7] is assumed; pure Spitzer resistivity would result in values for $\bar{Z}_\eta$, the effective ionic charge calculated from the resistivity, about 40% larger. We assume that the plasma is cylindrical, since the plasmas analyzed were not highly elongated. Uncertainties in the diagnostic data, especially in the profiles, introduce uncertainties of at least 30% in the calculated confinement times.

Results for divertor discharges with B_T = 17 kG, a = 38 cm, 'q_a' ≈ 3.1 and I_p ≈ 300 kA with a flattop time of 700 ms are shown in Figs. 5 and 6. The peak electron and ion temperatures were about 1 keV and 0.6 keV respectively. The confinement times for plasmas in the different divertor configurations in Fig. 2 appear to be similar but have not yet been extensively studied.

The electron confinement of D and H plasmas in PDX is comparable to the best achieved in PLT [8] with a ≈ 40 cm, I_p ≈ 400 kA and B_T = 32 kG. In helium discharges, confinement times are ~50% better: the electron temperatures are higher at the same or slightly lower loop voltages. Both the PDX and PLT discharges have confinement times significantly larger than the INTOR $\bar{n}a^2$ scaling law [9]. The PDX discharges are relatively clean with $\bar{Z}_\eta$ ≈ 1 for H and D even at relatively low densities, and $\bar{Z}_\eta$ ≈ 2 for helium.

Confinement times for circular and divertor configurations in PDX are very similar, but the $\bar{Z}_\eta$ for circular plasmas is higher, typically ≈ 2. Note that the gettering for circular discharges in PDX is not very effective since the getters evaporate in the remote divertor chambers and not in the central confinement region. In both divertor and circular discharges, the total energy confinement time including the ion energy approaches 80 ms.

4.3 Energy Balance. The plasma energy balance has been studied using a 19 channel bolometer array and thermocouple arrays on the neutralizer plates, as well as thermocouples on the limiters and other surfaces exposed to the plasma. Generally, circular discharges have ~40% of the input power radiated with ~25% of the input power absorbed on the limiter; the remaining power may be accounted for by radiation and charge exchange localized near the limiter. For divertor discharges, ~70% of the input power flows to the divertor with ~30% being radiated. Profiles of plasma radiation are shown in

Fig. 7 for a diverted discharge and two types of circular discharge. The first type is characterized by a flat radiation profile dominated by C and O radiation and sawtooth activity, the second by a peaked radiation profile due to titanium and m = 1 MHD activity without sawtooth oscillations. The power radiated from the central region ($r < 20$ cm) of the divertor plasma is ~10 kW, while for circular low-Z and high-Z plasmas the power is ~30 kW and ~60 kW respectively.

4.4 Impurities. Impurities are monitored with ultraviolet and soft x-ray spectrometers. Previous comparisons of impurity concentrations in circular and diverted discharges were made at low electron densities, $\bar{n}_e = 1.5 \times 10^{13}$ cm^{-3}, during early operation of PDX [2]. We have now extended the divertor/circular comparison to higher densities. All comparisons are made for discharges with the same I_p, B_T, $\bar{n}_e$ and R. The limiter radius was set at 42 cm for the circular discharges while the average separatrix radius was 38 cm for divertor discharges. The comparison of circular and diverted plasmas is complicated by differences in radiation profile and MHD activity between the two types of circular discharge as was discussed in Section 4.3, and by erratic bursts of Ti influx in the divertor discharges. The impurity contributions to the effective ionic charge $\bar{Z}_x$ determined from the soft x-ray pulse height spectrometer are given in Table I for divertor and circular discharges that have similar sawtooth activity. A complete UV spectroscopic survey of impurity concentrations was not available for these discharges, but rough indications of impurity behavior in the divertor and the two types of circular discharges can be obtained by comparing relative line intensities (Fig.8). In general, low-Z impurity emission for the two circular modes evolves roughly in the same manner until ~300 ms, at which time, for the sawtooth type discharge, the low-Z radiation

in the plasma periphery (e.g. CIII(977Å) and OIII(703Å)) increases by a factor of 5 to 10, while higher ionization stages of C and O (e.g. OVI(1032Å)) show much less, if any, change. This enhancement of low ionization state radiation near the edge without significant increases in high ionization state radiation from the center has been observed previously on PLT [8]. The diverted discharges have lower intensities than either type of circular discharge, e.g CIV(312Å) and CVI(34Å) are ~3 times lower in the diverted plasmas than in the circular cases while OVI(150Å) and OVII(22Å and 1623Å) are down by ~2.5. For the circular discharges characterized by m = 1 activity, TiXII(461Å) reaches a steady state level ~20 times higher than that in the diverted discharges. In the sawtooth circular case, TiXII(461Å) reaches a value about 2/3 that of the m = 1 case until the low-Z impurity radiation from the outer edge jumps up, after which the steady state intensity is ~3 times the level in the diverted discharges. Central titanium radiation (TiXIX(169Å)) during the steady state portion of the discharge is a factor of 10 - 15 less in the sawtooth discharges than in m = 1 circular discharges. There is a further decrease by a factor of 5 in the diverted plasmas compared with the sawtooth discharges. Equivalent reductions in central Ti densities cannot be inferred from this data due to relatively low $T_e(0)$ = 800 eV, which causes the TiXIX radiation to be sensitive to small changes in the ionization distribution in the plasma core. In general, the diverted plasmas are cleaner than the best circular discharges, and the divertor seems most efficient in reducing the high-Z impurity content while also producing a modest reduction in the low-Z elements. The random bursting of Ti in the divertor discharges mentioned earlier is not fully understood and can, at times, produce instantaneous levels of Ti emission from the plasma core which are comparable to typical clean circular discharges.

5.0 PRELIMINARY NEUTRAL BEAM INJECTION RESULTS

The first phase of the Joint ORNL/PPPL Heating Project has gone into operation on PDX. This initial system consists of two neutral beams, each with a rating of 1.5 MW at 50 keV with a 500 ms pulse length. The beams are oriented to inject 9° from perpendicular in the CO direction. The system has been operated at ~70% of full power for pulse lengths of 200 - 300 ms.

5.1 Typical Parameters During Beam Injection. A nominal 1 MW H^0 beam was injected into a deuterium plasma with $\bar{n}_e \simeq 3.4 \times 10^{13}$ cm^{-3}, $I_p \simeq 300$ kA, $a = 38$ cm, and $B_T = 17$ kG for circular, standard-Dee and inverse-Dee magnetic configurations. Qualitatively, the plasma behavior was similar for all three cases. Typical waveforms for injection into the Dee configuration (Fig. 9a) indicate good electron heating with no significant impurity buildup as evidenced by the drop in loop voltage and increase in plasma current. There is a tendency for the density to drop during neutral beam injection which is partially overcome by the gas feedback system increasing the gas feed in an attempt to maintain the preprogrammed $\bar{n}_e$ waveform. The electron temperature from the x-ray emission averaged over a chord through the plasma center (Fig. 9b) indicates T_e increasing from 700 to 950 eV. Abel inversion of 4 chord measurements, would give a central T_e of 1100 - 1300 eV during beam heating. Electron cyclotron emission (ECE) is not absolutely calibrated at the moment and is used mainly for the time evolution of T_e at the plasma center (Fig. 9b). The decrease in electron temperature during the ohmic heating phase from 200 to 400 ms, occurs as the density is increasing and does not represent a deterioration of confinement. During injection, ECE indicates a central temperature increase of ~60%. The sawtooth amplitude is large and its period increases from 8 to 16 ms during beam heating. Very limited Thomson

scattering data are available for these shots. However, under similar discharge conditions Thomson scattering has indicated that the central T_e increases from 600 to 1100 eV. Charge exchange and neutron emission both show the ion temperature increasing from about 450 to 800 eV during the beam pulse. After injection when both the gas flow and density decrease, the electron and ion temperatures increase.

The diagnostic data are somewhat preliminary, and each diagnostic is subject to uncertainties of at least 20%. Particular concerns are that both charge exchange and neutron emission are tail measurements while the x-ray deduced temperatures are subject to uncertainties in the Abel inversion.

5.2 Energy Balance During Beam Injection. The neutral beam power injected into PDX is not measured directly: a calorimeter in the beam line ~1 m in front of the PDX aperture is used to measure beam power and then previously measured transmission efficiencies are used to calculate the injected power. A 20% loss is caused by beam divergence while reionization by neutral gas in the duct and scrape-off is estimated to contribute a less than 5% loss. About 30% of the remaining beam power is not absorbed in the plasma at the densities in these experiments and is deposited on a beam dump on the inside wall of the vacuum vessel. Charge exchange losses of trapped beam ions are estimated to be between 5 and 15% of the trapped power depending on the model chosen for the neutral density profile. Thus, in the nominal 1MW injection experiments, where the calorimeter power was 1.13 MW, the power absorbed by the plasma was 600 ± 90 kW. During the period of beam injection the ohmic power input was ~180 kW.

It is premature to make a definite statement on the variation of confinement time with beam heating since there are sizeable uncertainties in the density and temperature profiles as well as the input power. The present data suggest that the confinement time remained constant within a factor of roughly 2 during beam injection.

6.0 ENERGY AND PARTICLE FLOW INTO THE DIVERTOR

The energy deposition on the neutralizer plates during a standard-Dee discharge was measured with a thermocouple array mounted on one pair of inner neutralizer plate [2]. The temperature profile from the thermocouples is in qualitative agreement with time-resolved infrared TV measurements of the neutralizer plate surface temperature. The energy deposition profile is peaked within 2 cm of the calculated separatrix location. The limiters and other baffles in the main plasma chamber, and the outer divertor plates have negligible energy deposition. Assuming toroidal and vertical symmetry these data indicate that 70 ± 10% of the input energy flows onto the neutralizer plates. Approximately 90% of the total power into the divertor flows onto the plate on the large major radius side. During operation with a single null configuration produced by moving an elongated-Dee plasma vertically, the power became evenly divided between the two plates.

Langmuir probes and microwave interferometers were used to measure the plasma parameters near the neutralizer plates. For a plasma with $\bar{n}_e \approx 3.3 \times 10^{13}$ cm^{-3}, probe measurements gave an electron temperature of ~10 eV and density of $4 - 7 \times 10^{12}$ cm^{-3} near the plates. Probe measurements across the field lines indicated broad density and temperature profiles with a line density of $2 - 4 \times 10^{13}$ cm^{-2}, in fair agreement with the microwave interferometer measurement of 4×10^{13} cm^{-2} across the divertor throat.

Measurements were also made with a single Langmuir probe in the outside scrape-off region on the equatorial plane. For the standard-Dee discharges, the density showed a plateau extending about 7 cm from the outer towards the inner separatrix on the large major radius side (see Fig. 2b). The plateau density was in the range $4 - 15 \times 10^{12}$ cm^{-3} with the range arising from uncertainty in the effective probe area. Outside the plateau, the density decreased exponentially with a characteristic distance of 1 - 2 cm. The electron temperature was ~8 eV at 1 cm outside the separatrix decreasing to ~5 eV in about 10 cm. In the case of inverse-Dee and circular plasmas, there was no plateau, but the temperature and density were of the same order as in the standard-Dee case.

Assuming a sheath model, energy flow to the neutralizer plates for a deuterium plasma is given by $h = 8nkTV_{i\parallel}\sin\theta$ where $V_{i\parallel}$ is the mass flow velocity parallel to $\underset{\sim}{B}$ and θ is the angle of $\underset{\sim}{B}$ to the surface [10]. Using $h = 30$ Wcm^{-2} from thermocouple data and $n = 7 \times 10^{12} cm^{-3}$ and $T = 10$ eV from probe measurements, we find $V_{i\parallel} \simeq 3 \times 10^{6}$ cm/s $\sim V_S$, where $V_S = [(T_i + T_e)/m]^{1/2}$. The particle flow into the divertor, ϕ_D can be evaluated from the average power, P_D, onto the neutralizer plates and the measured scrape-off temperature. For ohmically heated discharges with $P_D \sim 260$ kW, $\phi_D = P_D/8kT \sim 2 \times 10^{22}$ D^+/s. The standard-Dee diverted discharges require an inflow of 5×10^{21} D/s to maintain $\bar{n}_e = 3.3 \times 10^{13}$ cm^{-3}. From the gas inflow, ϕ_G and the divertor flow, ϕ_D, one can roughly estimate the recycling coefficient, to be $\alpha = 1 - (\phi_G/\phi_D) \sim 0.75$, subject to the large uncertainty in the measurement of ϕ_D.

6.1 Impurity Injection. The observed reduction of impurities in the presence of the divertor could be due to shielding of wall impurities by the divertor scrape-off or reduction of impurity generation and recycling within the main

plasma chamber. A series of preliminary experiments on impurity injection has been carried out to study these effects.

Shielding of the plasma from low energy particles was studied by sequentially injecting SiH_4 by gas puffing (E ≈ 1/40 eV, 20 ms pulse) and atomic Si by laser ablation (E ≈ 5 eV, 300 μs pulse) into the same discharge, thereby minimizing uncertainties due to variations in plasma profiles and atomic processes. For each source, we determined the time-integrated SiXII signal normalized to the number of atoms injected. The ratio of these normalized signals for the laser ablation and gas puffing was found to be ~8 in both divertor and circular discharges indicating possible selective screening of the low energy Si. The integrated SiXII 499Å intensity was used to estimate the total influx of Si into the plasma core from the laser ablation source. Within a factor of three, 1×10^{17} ions out of 1.6×10^{17} laser injected atoms reach the plasma core for both diverted and circular plasmas, indicating essentially no shielding for the energetic impurities.

Impurity content in the discharge also depends upon whether the impurities recycle. This is important because impurities are observed to have a finite lifetime (~20 ms) in PDX for typical conditions. During these experiments, the SiXII intensity background increased during Si or SiH_4 injection by at least a factor of 4 more in circular plasmas than in diverted plasmas, indicating that Si injected from previous pulses was recycling from the limiter.

6.2 Hydrogen Pellet Injection. Experiments in conjunction with the Oak Ridge National Laboratory Plasma Technology Group have begun using the single pellet gas driven injector previously employed on ISX [11]. The injector will be used to explore differences in fueling efficiency and particle confinement between gas puffing and pellet injection. Initial results indicate that the

pellet penetration of divertor discharges is consistent with the ablation model used to interpret ISX data [12].

ACKNOWLEDGEMENTS

The authors of this paper wish to express their appreciation to all the staff of the Princeton Plasma Physics Laboratory supporting the PDX project. Without their skill, dedication, perseverance and personal sacrifice the results reported here could not have been achieved.

We would also like to thank H. Haselton and W. Gardner of Oak Ridge National Laboratory for their excellent work in the development of the PDX ion sources and collaboration in the fabrication of the beam systems.

This work was performed under the United States Department of Energy Contract No. DE-AC02-76-CHO3073.

REFERENCES

[1] MEADE, D., ARUNASALAM, W., BARNES, C., BOL, K., COHEN, S., et al., Controlled Fusion and Plasma Physics (Proc. 9th European Conf. Oxford, 1979) 1, 91.

[2] OWENS, D.K., ARUNASALAM, W., BARNES, C., BELL, M., BOL, K., et al., "PDX Divertor Operation", 4th International Conference on Plasma Surface Interaction on Controlled Fusion Devices, April 1980, Garmisch-Partenkirchen F.R. Germany, to be published.

[3] WESSON, J.A., Nucl. Fusion 18 (1978) 87.

[4] McGUIRE, K., ROBINSON, D.C., WOOTTON, A.J., Plasma Physics and Controlled Nuclear Fusion Research (Proc. 7th Conf. Innsbruck, 1978) IAEA Vienna 1 (1979) 339.

[5] STOTT, P.E., HUGILL, J., FIELDING, S.J., McCRACKEN, G.M., POWELL, B.A., and PRENTICE, R., Controlled Fusion and Plasma Physics, (Proc. 8th European Conf. Prague, 1977) 1, 36.

[6] MURAKAMI, M., CALLEN, J.D., BERRY, L.A., Nucl. Fusion 16 (1976) 347.

[7] HIRSHMAN, S.P., HAWRYLUK, R.J., BIRGE, B., Nucl. Fusion 17 (1977) 611.

[8] HAWRYLUK, R.J., BOL, K., BRETZ, N., DIMOCK, D., EAMES, D., et al., Nucl. Fusion 19 (1979) 1307.

[9] Report on the International Tokamak Reactor Workshop, Vienna 1979 (International Atomic Energy Agency, Vienna 1980) p. 85.

[10] LOVBERG, R.H., in Plasma Diagnostic Techniques (eds. R. H. HUDDLESTONE AND S. L. LEONARD), Academic Press, London 1965, p. 69.

[11] MILORA, S.L., FOSTER, C.A., Rev. Sci. Inst. 50 (1979) 482.

[12] MILORA, S.L., FOSTER, C.A., EDMONDS, P.H., and SCHMIDT, G.L., Phys. Rev. Letters 42 (1979) 97.

TABLE I

Contribution to Z_{eff} in Ohmically Heated Deuterium Discharges from Soft X-ray Analysis

	Divertor (Standard-Dee)	Circular
$\bar{n}_e (10^{13}\ cm^{-3})$	3.4	4
$Z_{Chlorine}$	~.002	.02
$Z_{Titanium}$	~.004	.02
Z_{Oxygen}	.06	.19
Z_{Carbon}	.02	.07
$Z_{Hydrogen}$	.99	.96
$\bar{Z}_x$	1.08	1.3
$\bar{Z}_\eta$	1.06	1.9

FIGURE CAPTIONS

Fig. 1 Cross-section schematic of the PDX tokamak.

Fig. 2 Flux plots of MHD equilibria that have been obtained in PDX. In addition, these configurations can be displaced vertically to produce configurations asymmetric about the midplane.

Fig. 3 Measurements of the growth rate for vertical positional instability as a function of the major radius (i.e. field index). For these experiments midplane symmetric divertor coils were connected in parallel to provide passive stabilization. $I_{passive}$ is the current induced in the passive stablization circuit by vertical plasma motion.

Fig. 4 Operating parameters for PDX divertor discharges with a = 38 cm, and B_T = 17 kG. 'q_a' is the safety factor calculated assuming an equivalent circular plasma.

Fig. 5 Electron energy confinement time for ohmic discharges in a divertor configuration versus line average electron density. The discharge parameters were I_p = 300 kA, 'q_a' = 3.1, B_T = 17 kG and a = 38 cm. The PLT upper bound line represents the maximum electron energy confinement times achieved in PLT for $I_p \simeq 400$ kA, $q_\ell \simeq 5$, B_T = 30 kG and a = 40 cm [8].

Fig. 6 $\bar{Z}_\eta$ for ohmic discharges in a divertor configuration (except where noted) versus line average electron density. The discharge parameters were $I_p \simeq 300$ kA, 'q_a' $\simeq$ 3.1, B_T = 17 kG and a = 38 cm.

Fig. 7 Total radiated power and volume radiation profiles determined from a bolometer array for diverted and circular plasmas with I_p = 300 kA

and $\bar{n}_e = 3 \times 10^{13}$ cm^{-3}. The volume radiation profiles are at 500 ms. The ohmic power input was 300 and 375 kW for diverted and circular discharges respectively.

Fig. 8 Impurity line intensities for standard-Dee and two types of circular discharges in PDX.

Fig. 9a Typical waveforms during perpendicular injection into the standard-Dee configuration.

Fig. 9b Electron temperature variation during neutral beam heating.

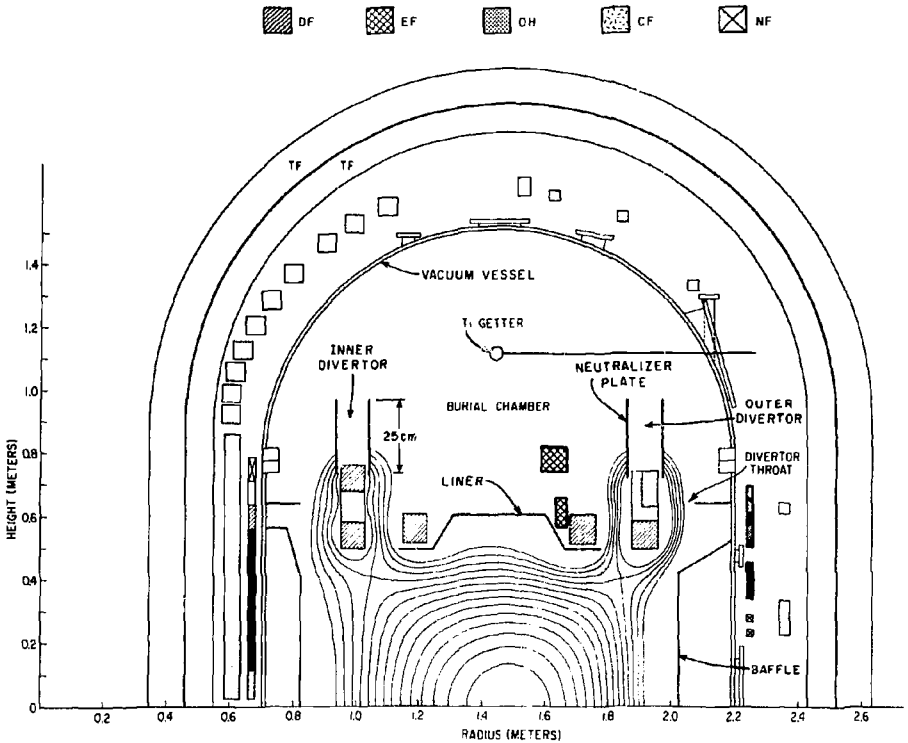

Fig. 1. (PPPL-803771)

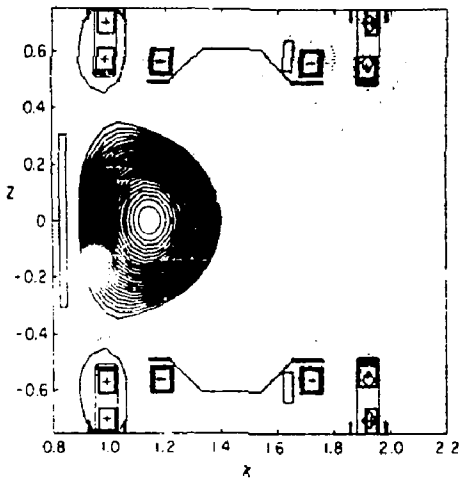

(a) Elongated Dee

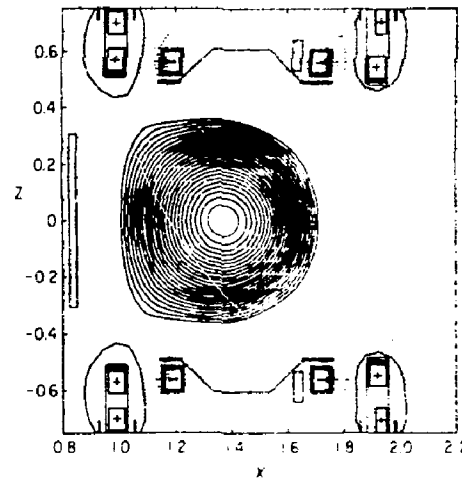

(b) Standard Dee

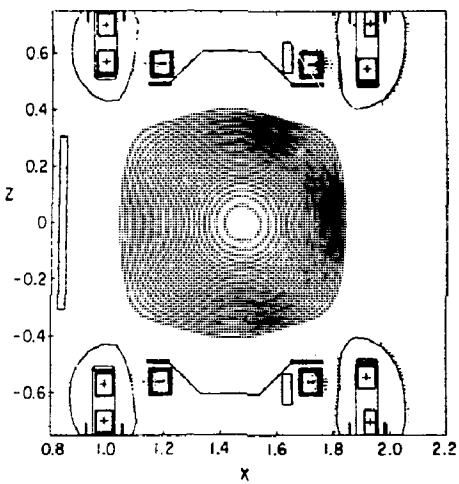

(c) Square

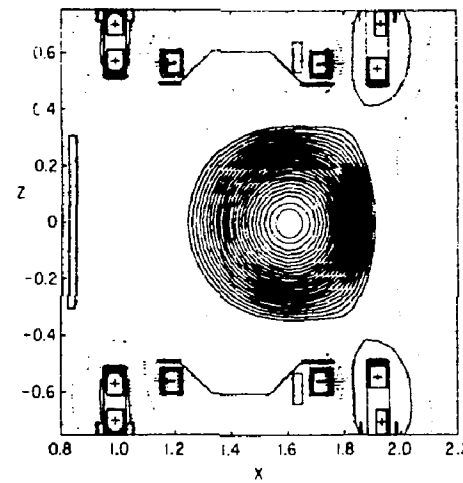

(d) Inverse Dee

Fig. 2. (PPPL-803950)

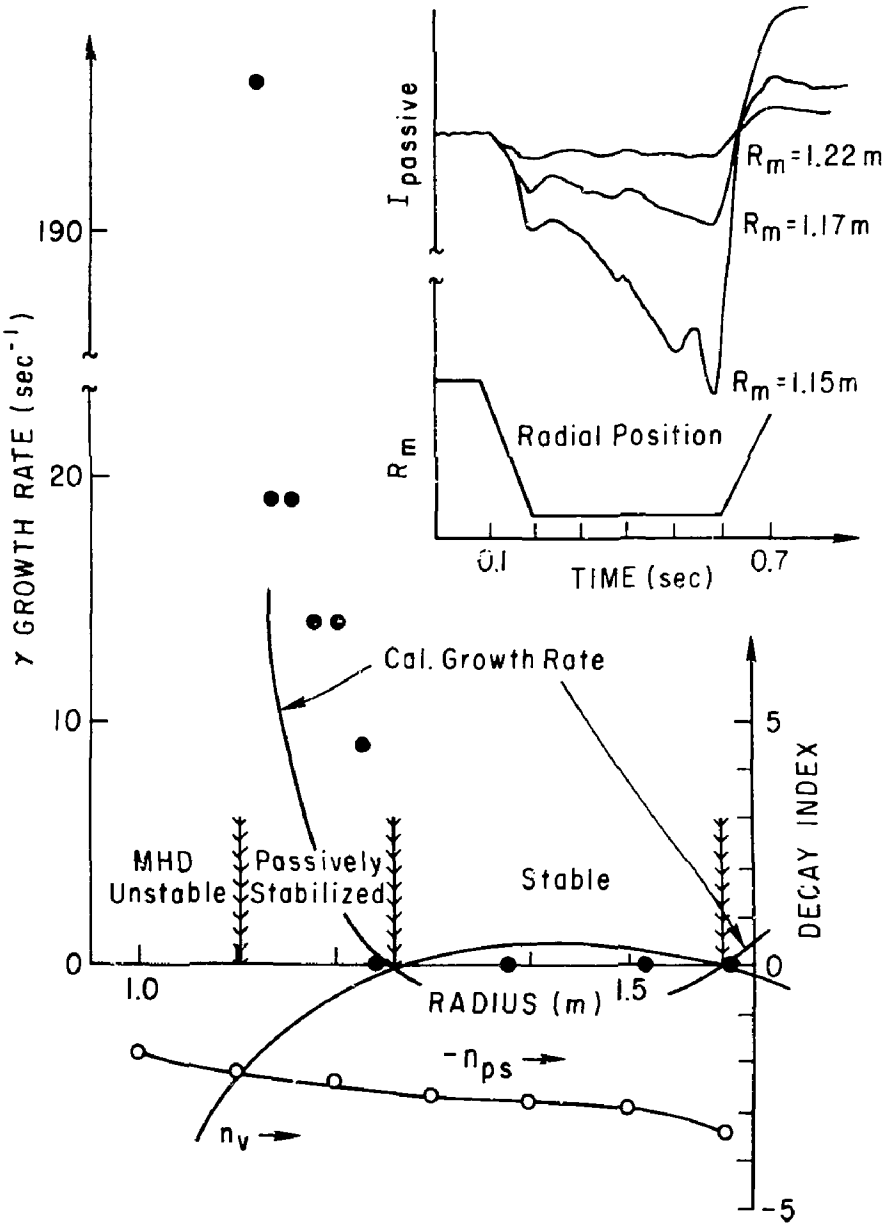

Fig. 3. (PPPL-803991)

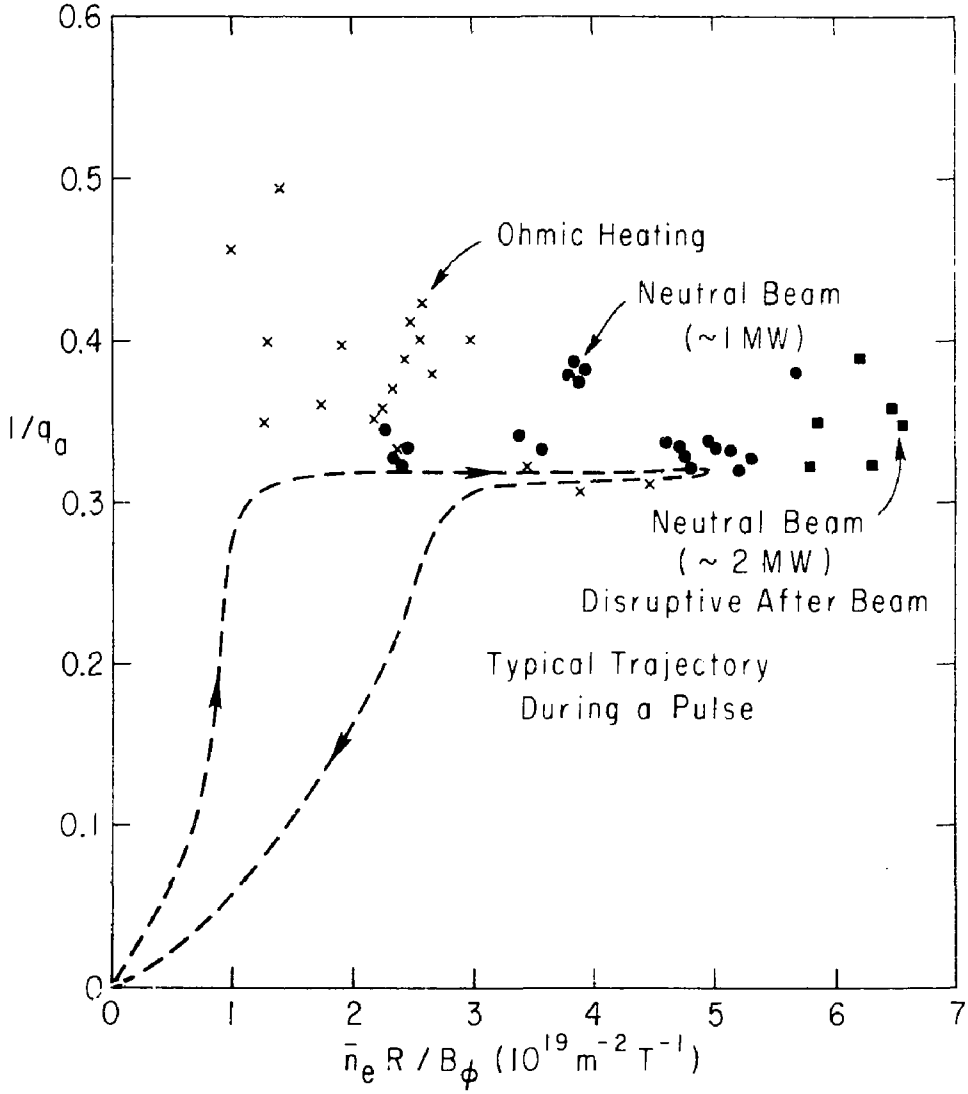

Fig. 4. (PPPL-803972)

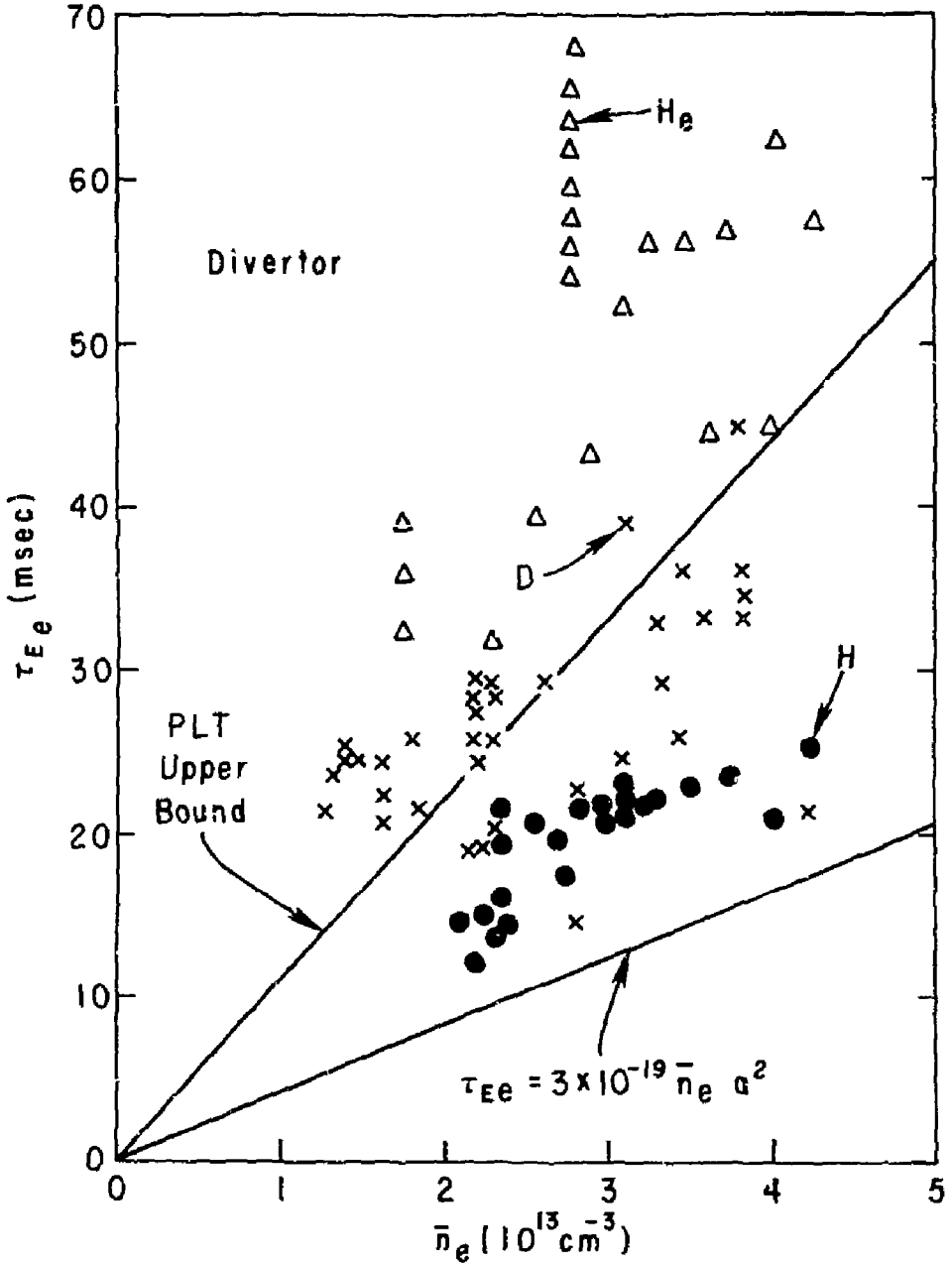

Fig. 5. (PPPL-803993)

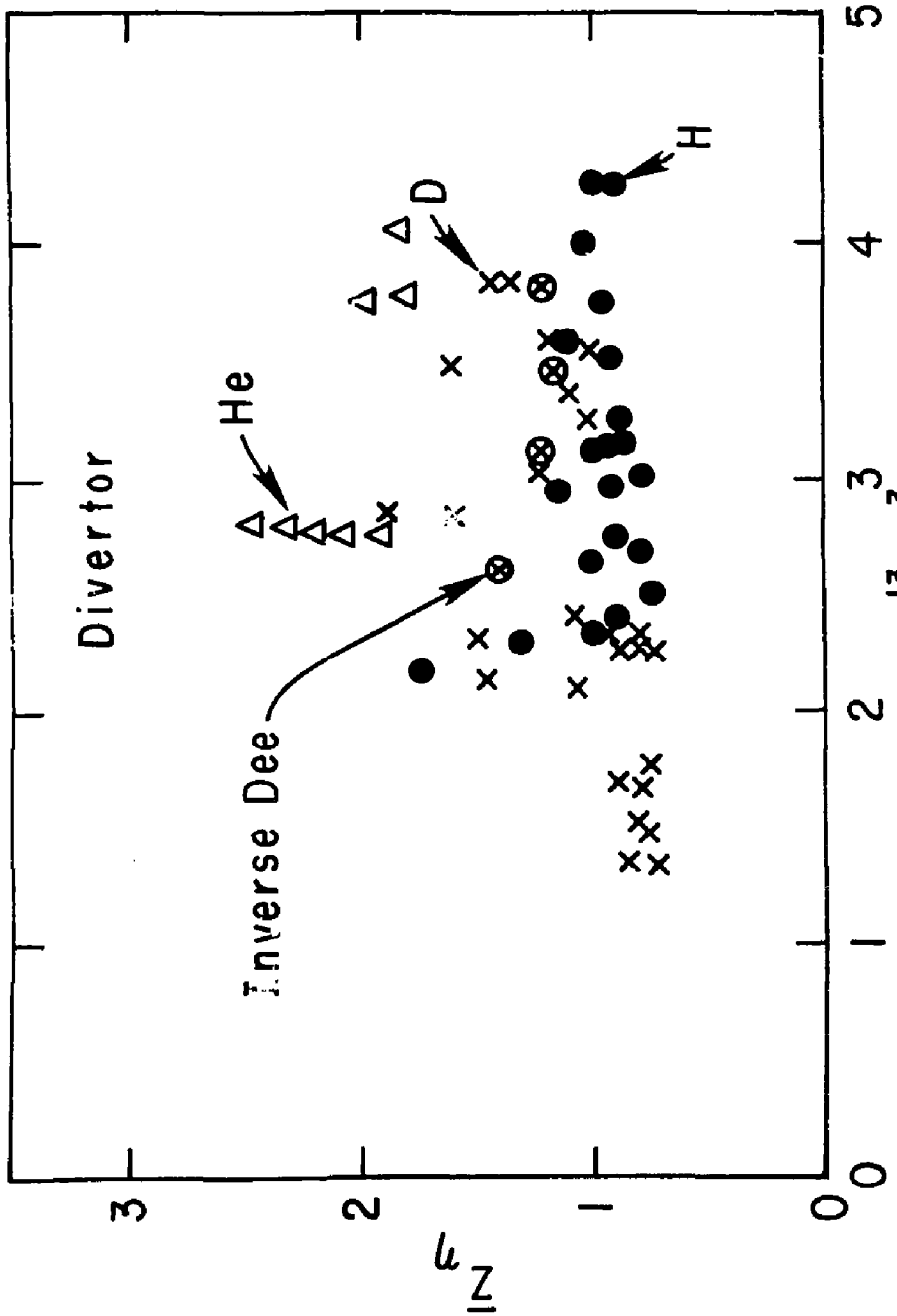

Fig. 6. (PPPL-803985)

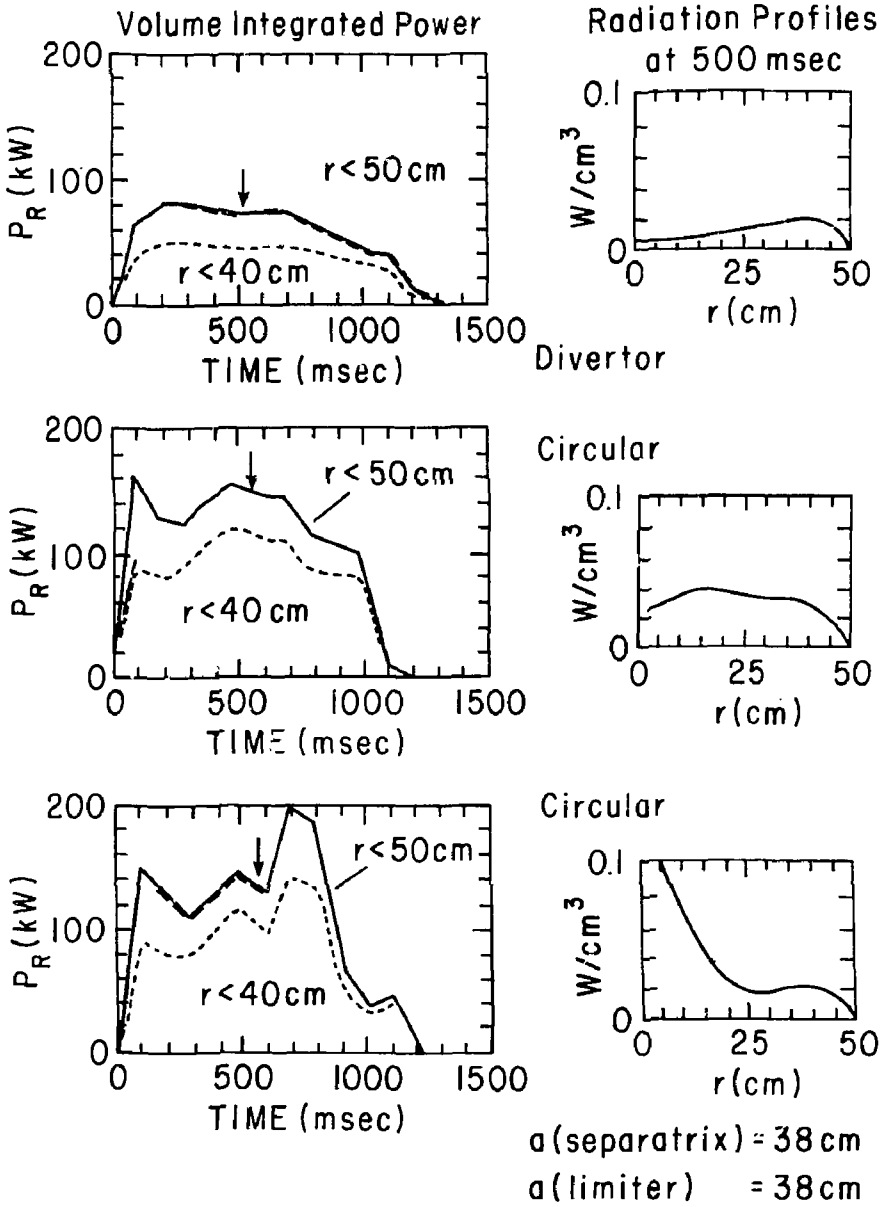

Fig. 7. (PPPL-806004)

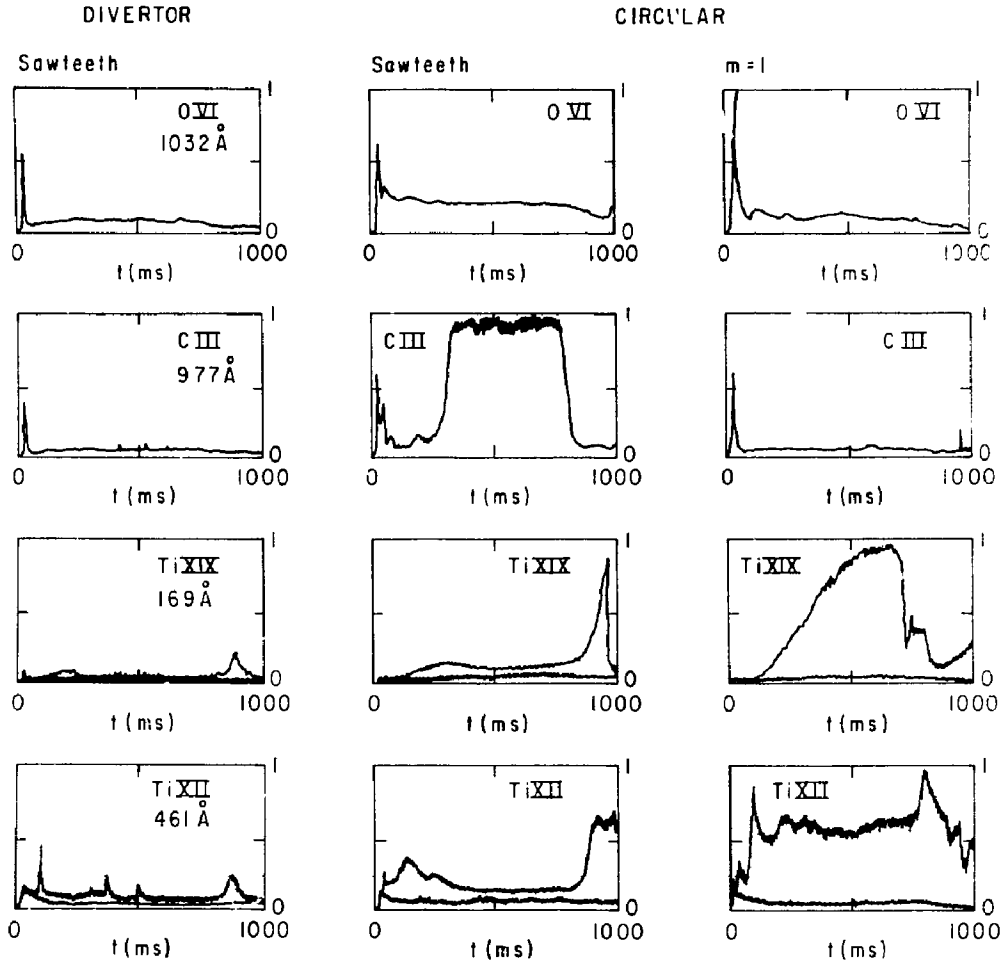

Fig. 8. (PPPL-806464)

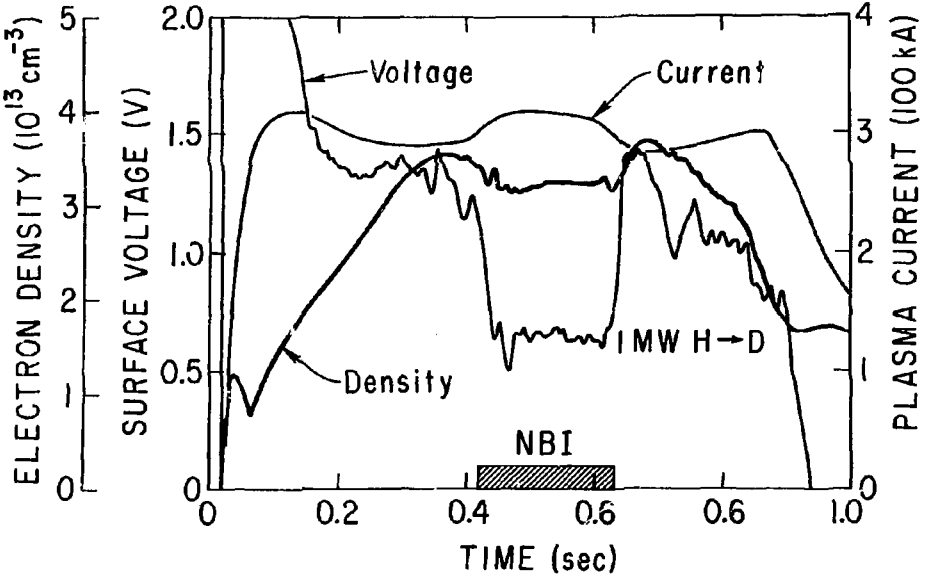

Fig. 9a. (PPPL-806000)

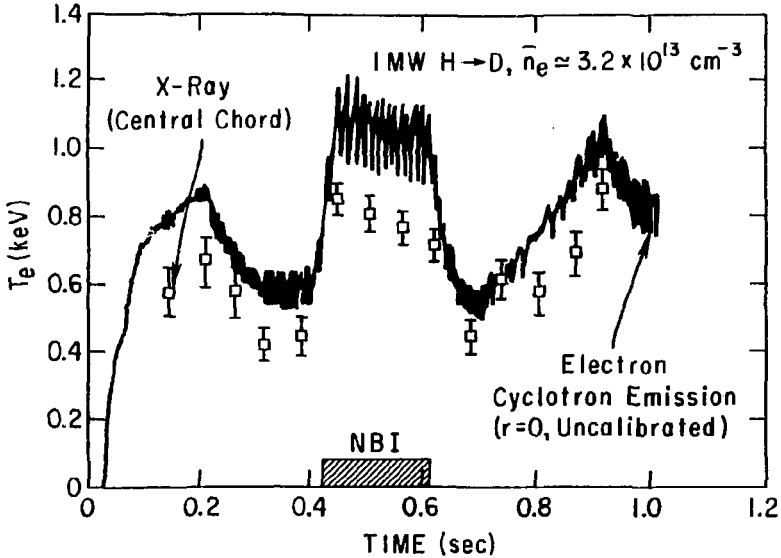

Fig. 9b. (PPPL-803998)